International Journal of Computational Intelligence and Informatics, Vol. 2: No. 2, July - September 2012

A New Speed Function for Level set Based Deformable Model for Tumor Segmentation in Medical Images

Somaskandan Suthakar
Department of Computer Science,
University of Jaffna,
Jaffna, Sri Lanka.

Sinnathamby Mahesan
Department of Computer Science,
University of Jaffna,
Jaffna, Sri Lanka.

***Abstract*-Tumor segmentation from medical image data is a challenging task due to the high diversity in appearance of tumor tissue among different cases. In this paper we propose a new level set based deformable model to segment the tumor region. We use the gradient information as well as the regional data analysis to deform the level set. At every iteration step of the deformation, we estimate new velocity forces according to the identified tumor voxels statistical measures, and the healthy tissues information. This method provides a way to segment the objects even when there are weak edges and gaps. Moreover, the deforming contours expand or shrink as necessary so as not to miss the weak edges. Experiments are carried out on real datasets with different tumor shapes, sizes, locations, and internal texture. Our results indicate that the proposed method give promising results over high resolution medical data as well as low resolution images for the high satisfaction of the oncologist at the Cancer Treatment Unit at Jaffna Teaching Hospital.**

Keywords-level set, tumor segmentation, speed function.

I. INTRODUCTION

Modern medical imaging devices, such as Magnetic resonance imaging (MRI) and computed tomography (CT) imaging play a crucial role in diagnosis, surgery, irradiation planning, medical research and visualization in tumor treatment. In radiotherapy it is necessary to precisely define the tumor lesions for irradiation to avoid irradiating healthy tissue. Radiation oncologists and many other medical experts spend a large amount of time in segmenting tumor volume in medical images. The task of image segmentation is actually the partition of an image into a number of non-overlapping regions, each with distinct properties.

In the past two decades, Geometric deformable models, or level set based deformable models, has found widespread application in many fields of medical image segmentation and has undergone immense development in terms of its theoretical insight, as well as making itself more flexible and adaptable. They were independently proposed by Caselles*et al.* [1] and by Malladi*et al.* [2]. The level set based deformable models can automatically handle topology changes in an image and allow for multiple simultaneous boundary estimations, and they are not sensitive to initial starting.

In this paper, to segment the tumor data, we proposed a level set based deformable model with a new speed function. Section III illustrates the proposed speed function in detail, and explains its role in the deformation process, whereas section II gives a brief account on basics of the classic speed function. Our method can even segment the tumors whose boundaries are not well defined.

II. THE CLASSIC SPEED FUNCTION

In their initial work, Caselles*et al.* [1] and Malladi*et al.* [2] proposed methods to solve the shape recovery problem by using the level set methods. They used an edge sensitive speed function of the form

$$F = k_I(F_A + F_G) \tag{1}$$

where, F_A is the advection term, independent of the geometry of the front, which controls the direction of movement of the moving front. The second term F_G is the part that depends on the geometry of the front, such as its local curvature. This term keeps the moving front smooth and differentiable during propagation [2].

The contour evolution is coupled with the image data through a multiplicative stopping term k_I, given as:

$$k_I = \frac{1}{1+|\nabla\{G_\sigma(x,y)*I(x,y)\}|^m} \tag{2}$$

where, $\nabla\{G_\sigma(x,y) * I(x,y)\}$ denotes the gradient of the input image $I(x,y)$ after Gaussian smoothing with standard deviation σ and mean 0, and m is a positive integer.

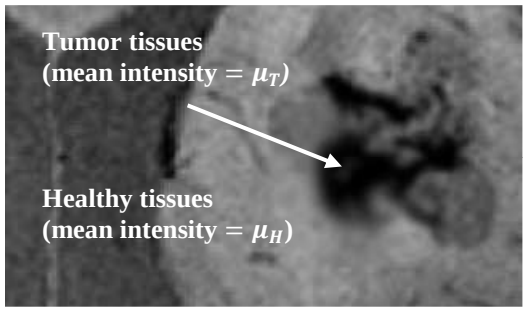

Figure 1: A hypointense tumor located in brain

In homogeneous regions, the term $\nabla\{G_\sigma(x,y) * I(x,y)\}$ will converge to zero, so that the effect of k_I on $F_A + F_G$ becomes negligible. If the boundary is well defined, at the boundaries the term $|\nabla\{G_\sigma(x,y) * I(x,y)\}|$ tends to infinity (*i.e.*, $F \to 0$), which stops the evolving front at the desired region and the final zero level set $\varphi = 0$ corresponds to the segmentation result.

While the strength of image gradient is a solid indicator of object boundaries, if the object boundary is indistinct or has gaps, the traditional deformable contour may leak out because the multiplicative term only slows down the curve near the boundary rather than completely stopping the curve.

Moreover, with the traditional speed function, the contours can only evolve in one direction, either inward or outward. If the curve passes the boundary, it will not be pulled back to recover the correct boundary.

III. An Improved Statistical Based Speed Function

Pure edge based methods offer accurate boundary localization, but need an extra propagation step to obtain completely closed region boundaries and usually do not have sufficient global knowledge to perform the task well. On the other hand, pure region based segmentation makes use of region statistics and can produce more semantically meaningful results, but typically suffers from poor localization of region boundaries. An ideal solution would perform global object segmentation with integrated region and edge information so that both region statistics and local edge responses can be utilized. Researchers have also been trying to integrate region and edge information in image segmentation [3][4][5][6].

Wang *et al*. [5] proposed a framework of deformable contour methods based on constrained optimization. They have integrated region and boundary information into one framework. Specifically, their strategy is to add the region information to the existing edge based level set formulation. They used an additional stopping term in terms of average brightness value and regional standard deviation. However, this method is still vulnerable to weak edges and gaps, and the resulting contours may either expand beyond the gaps or stops at noisy interiors [7].

Since region information is more global and less susceptible to noise, it will make the approach more robust and precise than the boundary based methods. A threshold-based scheme is proposed in [6], in which the level set speed function is designed using a global threshold. Motivated by these ideas, we have developed a new speed function with region information as well as the boundary based constraints.

A. A Statistical Model

A common statistical way of standardizing data on one scale so a comparison can take place is using a *Z-score*. A Z-score will describe how much a point deviates from a mean or specification point. Every normal random variable *X* can be transformed into a Z-score via the following equation:

$$Z = \frac{X-\mu}{\sigma} \tag{3}$$

where*X* is a normal random variable, μ is the mean of *X*, and σ is the standard deviation of *X*. Therefore, in other way, the above equation (3) can be used to determine a value for the random variable *X* for a given Z-score value.

Now, we will devise a model to segment the *hypointense* tumors, in which the tumor tissues appear as darker than the healthy tissues, as shown in Figure 1. In such cases, it can be safely stated that,

$$\mu_T < \mu_H \tag{4}$$

where μ_T and μ_H denote the mean intensities of the tumorous and healthy tissues respectively. For the *hyperintense* tumor images, the tumor tissues appear as relatively brighter than the healthy tissues, we can consider the inverted image so that the tumor area becomes darker and the same method can be applied.

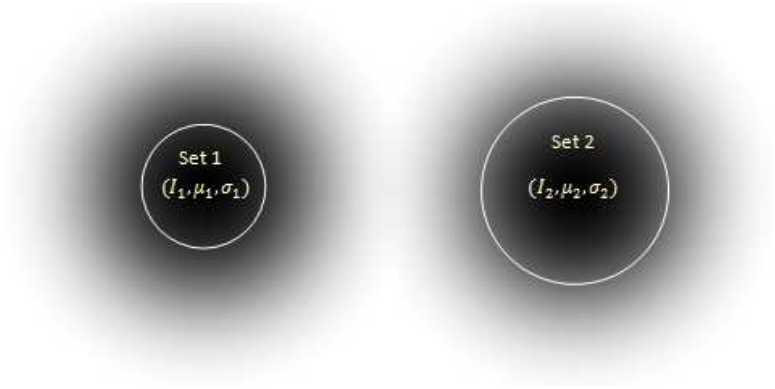

(a) Set-1 (I_1, μ_1, σ_1) (b) Set-2 (I_2, μ_2, σ_2)

Figure 2: Two sets of data from same image

Even though the above equation (4) is obvious, there might be some overlapping in the tumor and healthy voxels' intensity distributions, such as shown in the Figure 1. Therefore, it is difficult to segment a tumor by simply using only the gradient based speed functions.

Our approach is to let the manually placed contours to deform inside the tumor region towards the boundary. We roughly estimate the tumor's *maximum intensity level*I_T regularly using statistical measures. If there are any points on the moving contour whose intensity is nearly equal to I_T, such points are shifted slowly, while the other contour points can have much higher evolving speed. Once all the contour points reached the tumor boundary, the process will be terminated.

We have formulated an equation to calculate the tumor's maximum intensity level I_T in terms of the regional statistical information. Consider an image shown in Figure 2, in which the intensity is gradually increasing from the center (as usual, assume that the white's intensities are higher than the black's). Let I_1 and I_2 be random variables, and μ_1, σ_1 and μ_2, σ_2 be the respective mean and standard deviation of the regional intensities. Then, for a fixed Z-score value, it can be written as,

$$\frac{I_1-\mu_1}{\sigma_1} = \frac{I_2-\mu_2}{\sigma_2} \tag{5}$$

Since the set-1 has less brighter pixels than that of set-2, it is clear that the μ_1 would be less than μ_2. Similarly, it can also be stated that the σ_1 would be less than σ_2. Therefore, from the equation (5), it is obvious thatI_1 should be less than I_2. Hence, in general it can be stated that, if the contour expanded towards brighter region, then the corresponding *I* will be increased [8].

Now assume that the contour shown in Figure 2(b) is fixed, and hence, the corresponding μ_2 and σ_2 will be remain unchanged. In this case, using the equation (3), for various *Z* values we will get a range of *I* values. By choosing an appropriate *Z* value, it will be able to get the *I* as equal to the maximum intensity value for the contour region [8]. This is the important concept of the proposed tumor segmentation method.

Let the maximum possible intensity value for a tumor tissue be I_T, and take it as a random variable. Then, from the equation (3), the I_T can be defined by,

$$I_T = \mu_T + Z_T\sigma_T \tag{6}$$

where, μ_T, σ_T are represent the mean and the standard deviation of the tumor tissues respectively.

But the problem is neither the exact μ_T nor σ_T of the entire tumor region will be available at the initial stage of the deformation process. Therefore, we use the μ_T and σ_T of the initial contour/s for the rough estimation of the I_T. This estimation is then used to calculate the speed function, and the deformation of the zero level set will be carried out for one time step. New values for μ_T and σ_T can now be re-estimated. This process can be done repeatedly using the following iterative form of the equation (6):

$$I_T^n = \mu_T^n + Z_T^n\sigma_T^n \tag{7}$$

where $n \geq 0$, I_T^n denotes the approximate maximum limit for tumor intensity for the identified tumor voxels at the n^{th} step, and $n = 0$ corresponds to the initial stage. The μ_T^n andσ_T^n represent the mean and the standard

(a) Tumor in brain MRI (b) Unnecessary portions are croppedout (c) Identifying non tumor region

Figure 3: A rough selection for initiating the segmentation process

deviation of the tumor tissues respectively.

The appropriate selection of Z_T^n is another major problem. A simple technique is used in [6] to overcome this issue, and we have used it for our purpose. To eliminate the Z_T^n term, we will deduce another equation similar to the equation (6) by considering the healthy tissues' *minimum intensitylevel*,I_H:

$$I_H = \mu_H - Z_H \sigma_H \tag{8}$$

Where, μ_H and σ_H represent a rough estimations of the mean and the standard deviation of the healthy tissues respectively. Based on the equation (4), we know that $I_T^n \leq I_H, \forall n$. But, at the end of the segmentation process, both I_T^n and I_H should be identical. Moreover, according to the statistical concepts, we could take $Z_H$as Z_T^n. Then, by considering the equations (7) and (8), we could arrive at

$$I_T^n = \frac{\mu_T^n \sigma_H + \mu_H \sigma_T^n}{\sigma_H + \sigma_T^n} \tag{9}$$

Using this equation, the maximum intensity limit for the tumor region can be calculated as an iterative manner. For a rough estimation of the $\mu_H$and σ_H, we have to have information about at least some healthy voxels. A simple technique has been devised in our system to collect a set of healthy voxels, with minimal user intervention. Once the MRI image is loaded, the region other than a rectangular region which contains the tumor voxels is cropped out to reduce the unnecessary computational complexities. Then the user has to roughly distinguish between tumor and healthy tissues using two-level threshold function, which is illustrated by Figure 3. Using this information, a rough estimation of μ_H and σ_H will be determined only once, at the initial stage of the segmentation process.

B. The Speed Function

A good speed function has to push the zero level set $\varphi = 0$ faster at the homogeneous regions, has to maintain the smoothness of the zero level set $\varphi = 0$ while deforming, has to change the direction of evolution whenever needs, and has to stop the moving front at the boundaries. We have defined a speed function to achieve all these constrains [8], as

$$F = F_S \cdot g(I)(1 - \varepsilon k) \tag{10}$$

where, ε is a constant, and the k is the local curvature of the moving front. The term F_S is much like the advection term F_A used in the equation (1), but here, it determines the direction of movement dynamically, as well as controls the evolving speed based on the regional information. We use the same k_I from the equation (1) for $g(I)$, but the m is chosen as 1. That is,

$$g(I(x,y)) = \frac{1}{1+|\nabla\{G_\sigma(x,y) * I(x,y)\}|} \tag{11}$$

The term F_S has been devised based on the statistical model given in the equation (9), such that the speed value for a point on the zero level set $\varphi = 0$ is assigned according to the intensity difference between the particular point and the estimated minimum intensity for the tumor. If the difference is large, then the particular point is most likely to be well inside the tumor region. Hence, it can move faster. There might be some boundary voxels with very high intensities. For such cases, the stopping term $g(I)$ stops the front without any problem as the gradient will be very large.

Let I_T^n be the estimated minimum tumor intensity for n^{th} iteration, then the F_S of a particular point p on the contour C is defined as:

$$F_S^n(p) = \left(I_T^n - I_p\right)/|D^n| \tag{12}$$

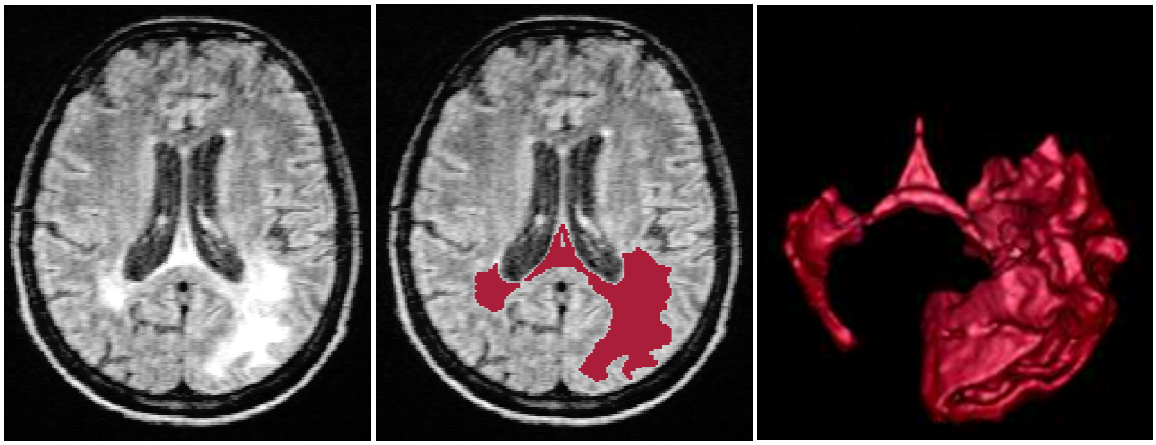

(a)a slice of a brain FLAIR MRI (b) Identified tumor region (c) 3D view of the segmented tumor

Figure 4. An example of the tumor segmentation.

where,

$$D^n = \begin{cases} max_{q\epsilon C}(I_T^n - I_q)\,, if I_T^n - I_p \geq 0 \\ min_{q\epsilon C}\left(I_T^n - I_q\right), if I_T^n - I_p < 0 \end{cases} \tag{13}$$

And the speed function, given in the equation (10), can be written in the iterative form, as

$$F^n = F_S^n \cdot g(I)(1 - \varepsilon k^n) \tag{14}$$

The definition of F_S ensures that its value will be always in the range of $[-1,1]$. If the difference $I_T^n - I_p > 0$, then it should be considered as a tumorous voxel. Hence, the F_S will be positive and the front moves further with a speed proportional to the difference. When $I_T^n - I_p < 0$, it is most likely a non-tumor voxel, so the value of the F_S will be negative and proportional to the difference, and hence the front tends to shrink. If the difference is small, then the point is most probably at the boundary of the tumor, and therefore the evolution speed will slow down.

At the sharp edges the difference $I_T^n - I_p$ will be large, but the gradient produce a much smaller value of $g(I)$ and it will stop the moving front. On the other hand, at the blur boundaries, the gradient will not be quite enough to stop the moving front. But the difference $I_T^n - I_p$ will be very low, and hence, the moving front tends to move very slowly. For such situations, if the estimated value of I_T^n remain more or less stable for a period of time, the corresponding point can be permanently mounted at that location.

The constant ε should be chosen carefully, so that the $(1 - \varepsilon k^n)$ will never be a negative value, and hence, it will not change the direction of evolution. Even if the moving front passed the edge, the sign of the F_S will automatically change to negative and the front will start to shrink to get back to the edge.

IV. Experimental Results and Analysis

An experiment had been conducted on fifteen image data obtained from the two main hospitals for cancer treatment in the Northern Province of Sri Lanka: Jaffna Teaching Hospital, and Base Hospital Thellippalai. The test images, applicable to the system of the study, contain data of tumors of different shapes, sizes, and intensities from two famous modalities, namely MRI and CT.

An example of the segmented tumor produced by our method is shown in Figure 4.Figure 4(a) shows a slice of a brain FLAIR MRI of dimensions $216 \times 256 \times 176$ with a resolution of $1mm^3$iso-voxels. The tumor was spread in both side of the brain, and it appears as comparably high intensity. The tumor region is successfully segmented by our proposed method, which is shown in Figure 4(b) and Figure 4(c).

To evaluate the success of a particular segmentation approach, it is common to use the segmentations obtained manually by experts as *ground truth data*. The results of our method were compared to manual delineation by medical physicists, who are responsible for the Cancer Treatment Unit at the Base Hospital Thellippalai and

Jaffna Teaching Hospital. To minimize the inter-expert variability, the weighted averages of the manually segmented results obtained by experts have been used as ground truths.

In this study, four most suitable metrics have been used to compare the results obtained by our segmentation

TABLE I: COMPARISON OF GROUND TRUTH DATA AND THE OUTPUTS PRODUCED BY THE SYSTEM

Image #	GT (mm3)	SM (mm3)	∩	∪	∩/∪ %	HMD	FNR	FPR	FNR-FPR	HD (mm)
Image01	92746	93164	92323	93587	98.6	0.014	0.46	0.91	-0.45	-0.45
Image02	109705	110498	109267	110936	98.5	0.015	0.40	1.12	-0.72	6.540
Image03	11740	11953	11740	11953	98.2	0.018	0.00	1.81	-1.81	6.000
Image04	56550	57732	56550	57732	98.0	0.020	0.00	2.09	-2.09	10.392
Image05	76013	76184	75927	76270	99.6	0.004	0.11	0.34	-0.22	6.077
Image06	16756	16874	16637	16993	97.9	0.021	0.71	1.41	-0.70	4.141
Image07	3486	3487	3486	3487	100.0	0.000	0.00	0.03	-0.03	0.938
Image08	3817	3804	3800	3821	99.5	0.005	0.45	0.10	0.34	1.781
Image09	75393	77364	75392	77365	97.4	0.026	0.00	2.62	-2.61	7.483
Image10	15481	15319	15319	15481	99.0	0.010	1.05	0.00	1.05	2.000
Image11	24529	25343	24424	25448	96.0	0.040	0.43	3.75	-3.32	4.472
Image12	97948	99708	97947	99709	98.2	0.018	0.00	1.80	-1.80	10.198
Image13	39634	40244	39346	40532	97.1	0.029	0.73	2.27	-1.54	10.770
Image14	8911	9000	8901	9010	98.8	0.012	0.11	1.11	-1.00	2.828
Image15	8381	8546	8381	8546	98.1	0.019	0.00	1.97	-1.97	4.000

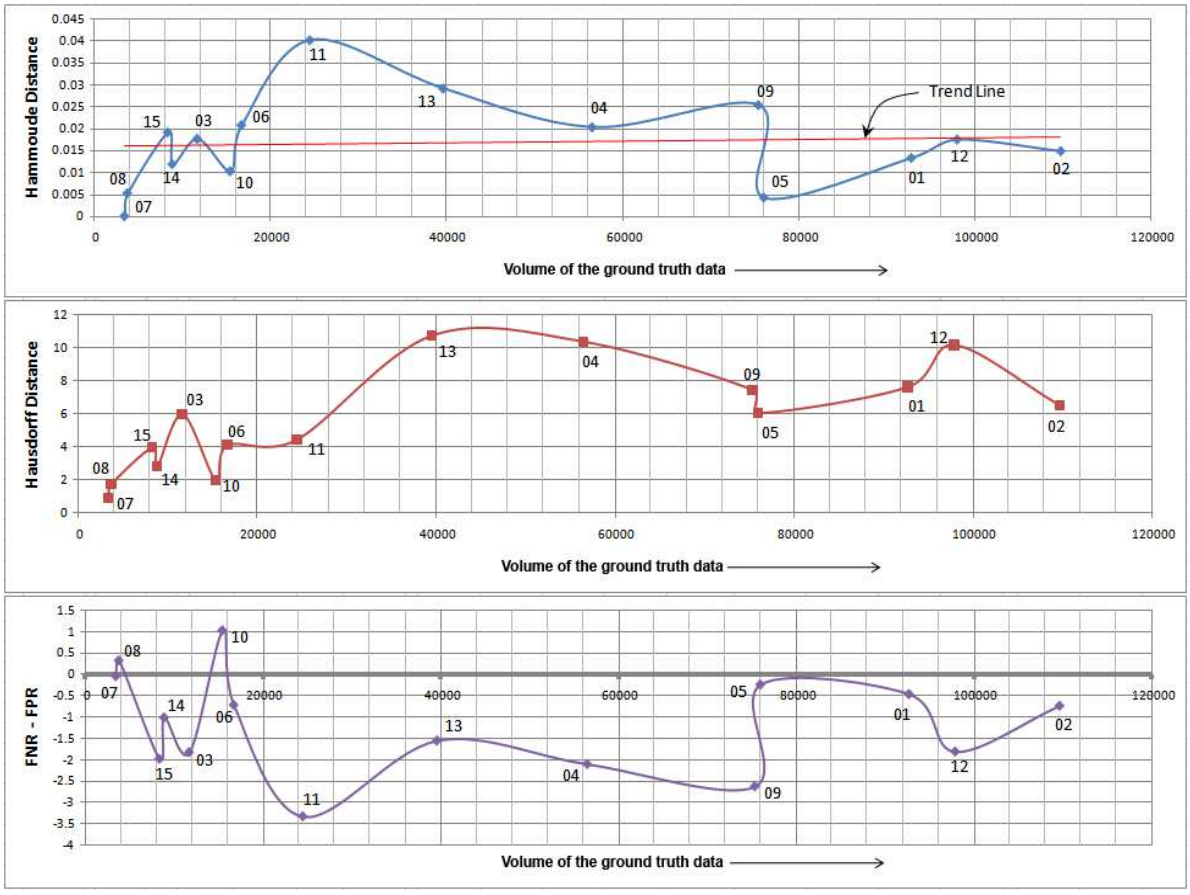

Figure 5: Comparison chart for ground truth and the outputs produced by the system

method (say SM) and the ground truth (say GT), which are given below:

- Hammoude Distance (HMD)

The Hammoude distance measures dissimilarity between sets of samples. It can be calculated by

$$HMD(SM,GT) = \frac{\#\left((SM \cup GT) \cap (\overline{SM \cap GT})\right)}{\#(SM \cup GT)}$$

where# denotes the number of voxels.

The HMD will be one if the two sets are disjoint, *i.e.*, they have no common members, and is zero if they are identical.

- False Negative Rate (FNR)

The false negative rate (FNR) measures the rate of pixels classified as lesion by the medical expert that were not classified as lesion by the segmentation method.

The measure of FNR is defined as follows

$$FNR(SM,GT) = \frac{\#(\overline{SM} \cap GT)}{\#(GT)}$$

- False Positive Rate (FPR)

The false positive rate (FPR) metric measures the rate of pixels classified as lesion by the segmentation method that were not classified as lesion by the medical expert.

The FPR is defined as follows

$$FPR(SM,GT) = \frac{\#(SM \cap \overline{GT})}{\#(GT)}$$

- Hausdorff Distance

The Hausdorff distance measures how far two subsets of a metric space are from each other, and which is defined as,

$$HD(SM,GT) = max\big(h(SM,GT), h(GT,SM)\big)$$

where,

$$h(P,Q) = \max_{p \in P} \min_{q \in Q} \|p - q\|$$

In Table I, the column 'GT' denotes the volume of the ground truth data and the column 'SM' denotes the volume of the corresponding segmentations obtained by the developed method.

Plots of Hammoude distances, Hausdorff distances, and the $FNR - FPR$ against the volume of the ground truth data are shown in Figure 5.The graph of Hammoude distance against volume shows that the volumetric overlap error is being below 0.03, except only one instance. In other words, 97% or above volumetric match were obtained except a single case. Another important point can be noted that the trend line in Hammoude distance against volume graph stretches out almost in the horizontal direction. This aspect guarantees that the accuracy of the segmentation method will remain stable even for large tumor volumes.

In the Hammoude distance against volume graph, the maximum error value corresponds to Image11. But the same Image11 has very low $FNR - FPR$ value, which can be observed in the $FNR - FPR$ against the volume graph. Hence, the possible reason for the higher Hammoude distance for this image would be that our method might have identified more voxels than the manually segmented result as tumorous lesions. Clinically, it is far better than missing tumor lesions. If we look at the graph of Hausdorff distances against the volume for the Image11, it has a quite lower value (*i.e.*, 4.472) than the average of 5.685. This means that the zero level set did not go beyond 4.472 mm from the ground truth data, and the excess voxels might have been collected within this distance.

One of the peek error values (*i.e.*, 10.392 mm) corresponds to Image04 in the Hausdorff distances against the volume graph. But it has one of the lowest values in the graph of $FNR - FPR$ against the volume, and it has a very good matching percentage of 98% in the Hammoude distance against volume graph. Hence, it can be guessed that the zero level set might have gone 10.392 mm away from the ground truth data along a thin branch of voxels, while rest of the tumor volume were identified accurately.

If we consider the $FNR - FPR$ against the volume plot, most of the section of the graph lies far below the x-axis. This means that our method's false negative detection rate is much less than the false positive detection rate. As mentioned before, a bit higher false positive rate has no harm in clinical point of view than false negative rate. If we look at the *FNR* at the table, for four cases among fifteen test images, our method did not miss even a single tumor voxel. In more than 50% of the test images, the false negative rate is very close to 0.1 or less.

As an overall view, our system has a very good volumetric matching percentage with very low false negative rate, and has an acceptable range of Hausdorff distance error rate. The presented experimental results on fifteen different data sets show that our method produces reliable results.

Moreover, it is worth mentioning the time factor at this juncture. Among the fifteen test images, the maximum time taken for producing the output has been found to be not more than three minutes, whereas the manual segmentation for the image that needed the maximum time for the system, took well around three hours. The personnel from the Cancer Treatment Unit at the Base Hospital Thellippalai and Jaffna Teaching Hospital are impressed by this factor too.

V. CONCLUSION

A new level set based deformable model for tumor segmentation has been presented. In the past two decades, Geometric deformable models have been found widespread application in many fields of medical image segmentation.

The classical edge-based level set methods are not suited to tumor segmentation as they are not discriminative enough when the appearance of tumor and normal tissue overlap. On the other hand, pure region-based segmentation makes use of region statistics and can produce more semantically meaningful results, but typically suffers from poor localization of region boundaries. Therefore, in the proposed work, the regional statistical measures are integrated into the gradient based speed function so that the deforming contour would not miss even the blurred boundaries. The gradient term in the speed function is responsible to stop the moving contour at strong edges. On the other hand, the regional statistical measures are used to identify weak and discontinued boundaries. The deforming contours handle the topological changes naturally and expand or shrink as necessary, and automatically identify the tumor voxels with high precision.

Quantitative analyses have been carried out by using fifteen different data sets. The segmented data were compared with ground truth data, and the results of the experiments show that the method produces reliable and promising results. The developed system has been checked by the medical physicists who are responsible for the cancer treatment planning at the base hospital Thellippalai and Jaffna teaching hospital. They expressed great satisfaction of the results produced by the system and their appreciation give us more confidence that our method works with high accuracy for the use of the cancer treatment unit, which would decrease the time from several hours to a few minutes in segmenting the tumor region.

ACKNOWLEDGMENT

We would like to thank Mr. J. Jeyasugiththan, medical physicist from Cancer Treatment Unit at Thellippalai Hospital, and Dr. N. Jeyakumaran, oncologist from Cancer Treatment Unit at Jaffna Teaching Hospital, for providing us with real medical images for our research, and for spending hours of time in evaluating our system.

REFERENCES

[1] Caselles, V., Catté, F., Coll, T., and Dibos, F., "A geometric model for active contours in imageprocessing," NumerischeMathematik, vol. 66, no. 1, pp. 1-31, 1993.

[2] Malladi, R., Sethian, J.A., and Vemuri, B.C., "Shape modeling with front propagation: a level set approach," IEEE Transactions on Pattern Analysis and Machine Intelligence (TPAMI), vol. 17, no. 2, pp. 158-175, 1995.

[3] Tian, Y., Duan, F., Zhou, M., and Wu, Z., "Active contour model combining region and edge information," Machine Vision and Applications, pp. 1-15, 2011.

[4] Tsechpenakis, G., and Metaxas, D. N., "CRF-driven Implicit Deformable Model," in CVPR, 2007, pp. 18-23.

[5] Wang, X., He, L, and Wee, W. G., "Deformable Contour Method: A Constrained Optimization Approach," International Journal of Computer Vision, pp. 87-108, 2004.

[6] Taheri, S., "Level-set segmentation of brain tumors in magnetic resonance images," Master's Thesis, National University of Singapore, 2008.

[7] Wang, X., Gao, F., and Wee, W. G., "Mean Field Annealing Deformable Contour Method: A Constrained Global Optimization Approach," in ICARCV, 2006, pp. 1-8.

[8] Suthakar, S., Mahesan, S., "A Level Set Based Deformable Model for Segmenting Tumors in Medical Images", Proceedings of the International Conference on Pattern Recognition, Informatics and Medical Engineering (PRIME-2012), pp. 280-285, 978-1-4673-1039-0. 2012.